Analysis Note: Measurement of symmentric cumulant in Au+Au collision at 39 and 200 GeV

MD NASIM

CONTENTS

LIST OF FIGURES

LIST OF TABLES

ABSTRACT

The analysis details of the symmetric cumulant measurement in Au+Au collisions at $\sqrt{s_{NN}}$= 39 and 200 GeV are presented in this note.

1 DATA SETS AND EVENT SELECTION CUTS

The results presented in this note are based on data collected from Au+Au collisions at $\sqrt{s_{NN}}$= 39 and 200 GeV with the STAR detector for minimum bias trigger in the years of 2010 and 2011, respectively. The minimum-bias trigger condition was based on a coincidence of the signals from the zero-degree calorimeters, vertex position detectors, and/or beam-beam counters. Total number of events analyzed for 0-80% centrality is about 110 and 400 Million after all event selection cuts for 39 and GeV, respectively. The events were selected within the vertex range $\pm$ 30 (40) cm in the Z (beam) direction for 200 (39) GeV. In addition, less than 2 cm cuts on vertex radii were applied to remove contamination from beam pipe. Figure 1 shows the distribution of uncorrected reference multiplicity and Z position of vertex in Au+Au collisions at $\sqrt{s_{NN}}$ =39 and 200 GeV. Centrality selection was done using StRefmultCorr Class and all bad runs listed in the StRefmultCorr Class are rejected from the analysis. Details of centrality selection study can be found at:http://www.star.bnl.gov/protected/common/common2011/centrality/200GeV/index.html and http://www.star.bnl.gov/protected/common/common2010/centrality/

2 TRACK SELECTION CUTS

Time Projection Chamber (TPC) with full 2π coverage was used for tracking in the central region ($\eta < 1.0$). The basic cuts for track selection is listed in the table 1.

* *Department of Physics and Astronomy, University of California-Los Angeles*

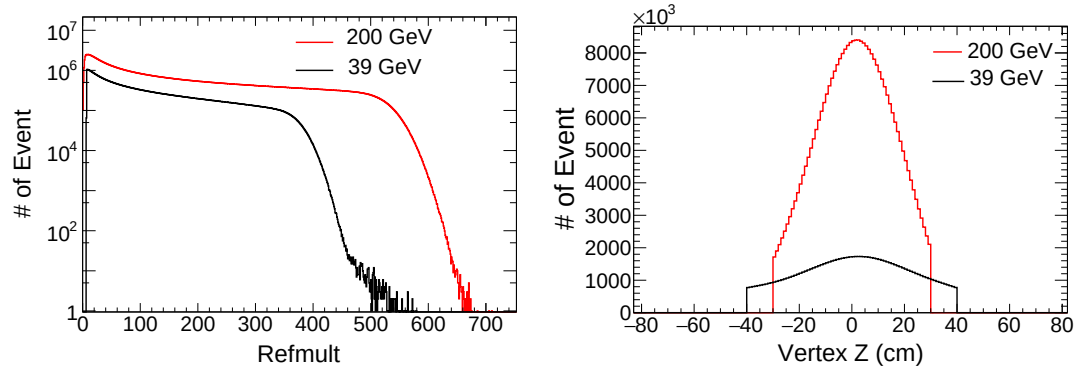

Figure 1: Left: The uncorrected multiplicity distribution of reconstructed charged particles. Right: Z-coordinate of primary vertex

Table 1: List of track selection cuts

Variable	Values
Number of fit points	$\geqslant 15$
Ratio of fit points to possible points	$\geqslant 0.51$ and $\leqslant 1.02$
Dca	<3 cm
p_T cuts	0.2 - 2.0 GeV/c
η cuts	± 1

3 ANALYSIS TECHNIQUE

Correlations between different order flow harmonics are predicted to be sensitive to the transport properties of the produced medium in heavy-ion collisions. Recently, a new tool, namely 4-particle symmetric cumulants [1], is emerging with a promise to throw additional light on the initial-state phenomena and the transport properties of the produced medium in heavy-ion collisions [2, 3, 4] . In this paper, we study the relationship between event-by-event fluctuations of magnitudes of two different flow harmonics of order n and m by using a recently proposed 4-particle observable [1]:

$$\begin{aligned}\langle\langle\cos(m\varphi_1+n\varphi_2-m\varphi_3-n\varphi_4)\rangle\rangle_c &= \langle\langle\cos(m\varphi_1+n\varphi_2-m\varphi_3-n\varphi_4)\rangle\rangle \\ &\quad - \langle\langle\cos[m(\varphi_1-\varphi_2)]\rangle\rangle\,\langle\langle\cos[n(\varphi_1-\varphi_2)]\rangle\rangle \\ &= \left\langle v_m^2 v_n^2\right\rangle - \left\langle v_m^2\right\rangle\left\langle v_n^2\right\rangle , \end{aligned} \tag{1}$$

3.1 Method

The azimuthal distribution (ϕ) of particles in a given event is written as

$$P(\phi) = \frac{1}{2\pi}\sum_{n=-\infty}^{n=+\infty} V_n e^{-in\phi}, \tag{2}$$

where $V_n = v_n e^{in\psi_n}$ is the n^{th} harmonic anisotropic flow coefficient with respect to event plane angle ψ_n. The 4-particle symmetric cumulants $SC(n,m)$ with $n \neq m$ [1] can be defined as

$$SC(n,m) \equiv \langle v_n^2 v_m^2 \rangle - \langle v_n^2 \rangle \langle v_m^2 \rangle. \tag{3}$$

Normalized symmetric cumulants $NSC(n,m)$ is defined as

$$NSC(n,m) \equiv \frac{\langle v_n^2 v_m^2 \rangle - \langle v_n^2 \rangle \langle v_m^2 \rangle}{\langle v_n^2 \rangle \langle v_m^2 \rangle}. \tag{4}$$

Magnitude of $NSC(n,m)$ gives correlation strength between $\langle v_n^2 \rangle$ and $\langle v_m^2 \rangle$.

The magnitude of $v_n^2 v_m^2$ and v_n^2 in the numerator of Eq. 4 is calculated using multi-particle cumulant method [1] as shown below.

$$\begin{aligned} v_n^2 v_m^2 &= \frac{1}{\binom{M}{4}4!} \sum_{\substack{i,j,k,l=1 \\ (i\neq j\neq k\neq l)}}^{M} e^{i(m\varphi_i + n\varphi_j - m\varphi_k - n\varphi_l)} \\ &= \frac{1}{\binom{M}{4}4!} \big[|Q_m|^2 |Q_n|^2 - 2\mathfrak{Re}\left[Q_{m+n} Q_m^* Q_n^*\right] \\ &- 2\mathfrak{Re}\left[Q_m Q_{m-n}^* Q_n^*\right] + |Q_{m+n}|^2 + |Q_{m-n}|^2 \\ &- (M-4)(|Q_m|^2 + |Q_n|^2) + M(M-6)\big], \end{aligned} \tag{5}$$

and

$$v_n^2 = \frac{1}{\binom{M}{2}2!} \sum_{\substack{i,j=1 \\ (i\neq j)}}^{M} e^{in(\varphi_i - \varphi_j)} = \frac{1}{\binom{M}{2}2!} \big[|Q_n|^2 - M \big]. \tag{6}$$

Where M is the multiplicity of an event and Q_n is flow vector for n^{th} harmonic, $Q_n \equiv \sum_{k=1}^{M} e^{in\varphi_k}$. The weights of $M(M-1)$ and $M(M-1)(M-2)(M-3)$ are used to get the event-averaged 2-particle and 4-particle correlations. Additional weights were also applied to correct the multi-particle correlation functions for the p_T-dependent efficiency (shown in Fig 2) and for imperfections in the detector acceptance. The magnitude of $\langle v_n^2 \rangle$ in the denominator of Eq. 4 is obtained with 2-particle correlations and using a pseudorapidity gap of $|\Delta\eta| > 1.0$ to suppress biases from few-particle non-flow correlations.

3.2 Non-Uniform Acceptance (NUA) Correction

To remove acceptance correlations from an imperfect detector, one must first make the Q-vector in Eqs. 5 and 6 isotropic in the laboratory. Two methods have been used to correct for non-uniform acceptance.

1. Phi Weighting - one weights each particle with the inverse of the azimuthal distribution of the particles averaged over many events.

2. Recentering - one subtracts from the Q-vector of each event, the Q-vector averaged over many events. In this analysis, Recentering correction has been applied for each track instead of on each event.

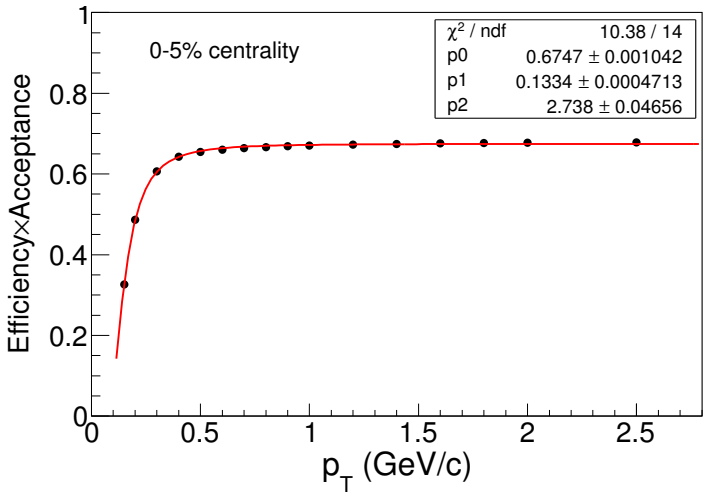

Figure 2: Charged hadron efficiency in Au+Au collision at 39 GeV

The Phi Weighting method is more intuitive, while the Recentering is more practical because it guarantees zero average Q-vector. Difference in results after applying both method has been taken as a source of systematic error. Both Recentering and Phi Weighting correction has been applied separately for each Run and Centrality. Distribution of Q-vectors (Q2, Q3 and Q4, just for example) is shown in Fig. 3 on the following page after applying correction for non-uniform acceptance.

Fig 4 shows ϕ angle distribution at 39 GeV before and after phi-weight correction.

After NUA correction, we have cross-check our analysis macro by reproducing published v2 (using 2-particle correlation method). Fig. 5 on page 7 shows comparison between our calculation and published results. One can see a very good agreement between this two results.

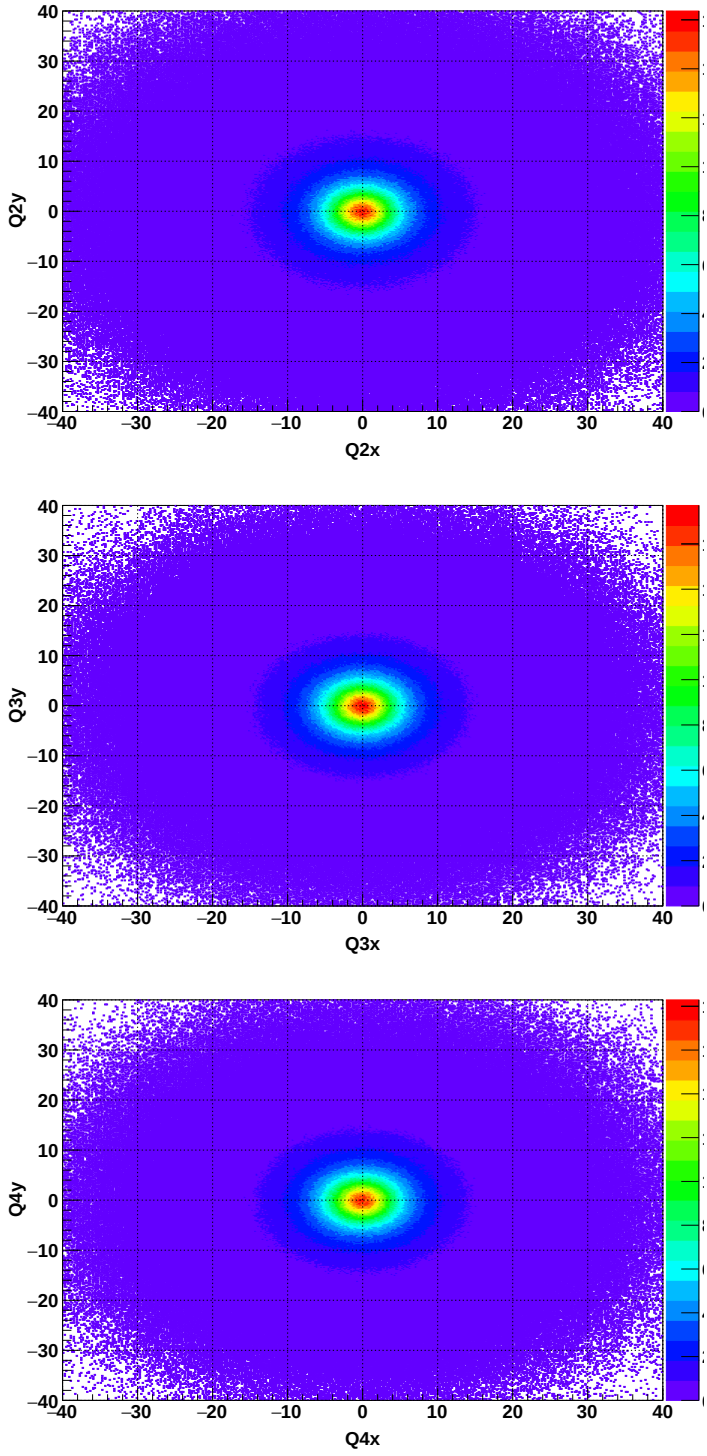

Figure 3: Example plots for Non-Uniform Acceptance corrected Q vector

3.3 Centrality Bin-Width (CBW) Correction

Experimentally, the centrality is usually determined by an observable like the charged particle multiplicity and the smallest centrality bin is determined by a single multiplicity value. Generally, experiments report the results for a wider centrality bin, such as 0-5%, 5-10% etc., to suppress the statistical fluctuations. It was point out in

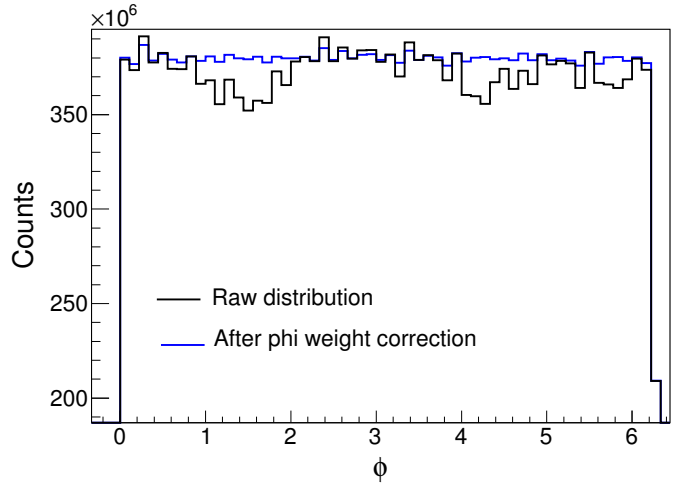

Figure 4: ϕ angle distribution at 39 GeV

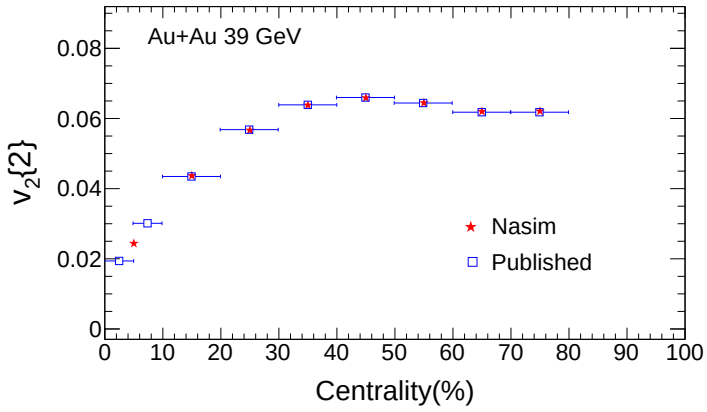

Figure 5: The elliptic flow using 2 particle correlation method has been reproduced to check analysis code and NUA correction.

Ref. [5] that significant biases can appear when using wide centrality bins. To reduce the centrality bin width effect, we have used a technique, called Centrality Bin Width Correction (CBWC), to calculate the various cumulants for each multiplicity in one wide centrality bin. The method has the weighted averaged by the number of events in each multiplicity. Fig. 6 on the following page shows SC(2,3) and SC(2,4) as a function of centrality in Au+Au collision at 200 GeV in 8 and 16 centrality bin after CBW correction. One can see the magnitude of SC variable is independent of centrality bin width.

4 SYSTEMATIC ERROR STUDY

The main sources of systematic uncertainty are followings: 1) Systematic due to event and track selection cuts and 2) Systematic due to non-uniform acceptance correction. List of cuts varied for systematic estimation is shown in Table 2. Systematic error

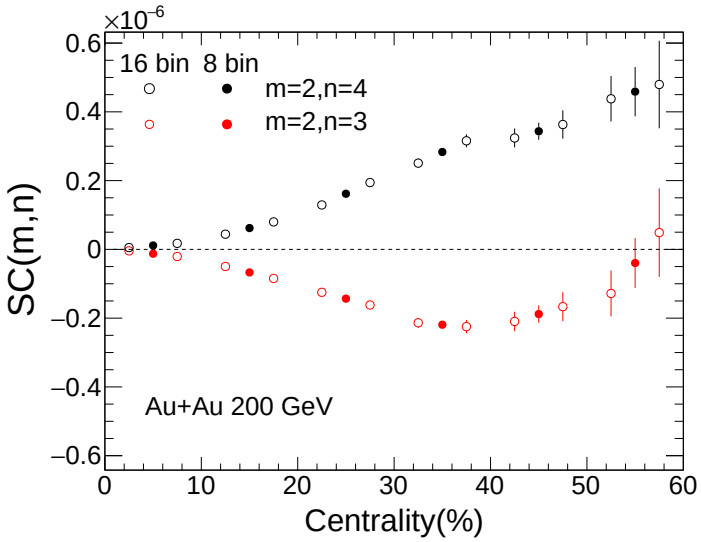

Figure 6: SC(2,3) and SC(2,4) as a function of centrality in Au+Au collision at 200 GeV in 8 and 16 centrality bin after CBW correction.

on SC(2,4) at 200 GeV from different sources are shown in Fig. 7. Total systematic error was obtained by adding errors in quadrature from different sources. Maximum systematic is from NUA correction method.

Table 2: List of cuts variation

Vz	Vr	Dca	Nhits	NUA Correction
±10 cm	2 and 1.5 cm	3 and 2 cm	15 and 20	ϕ weight and Recentering

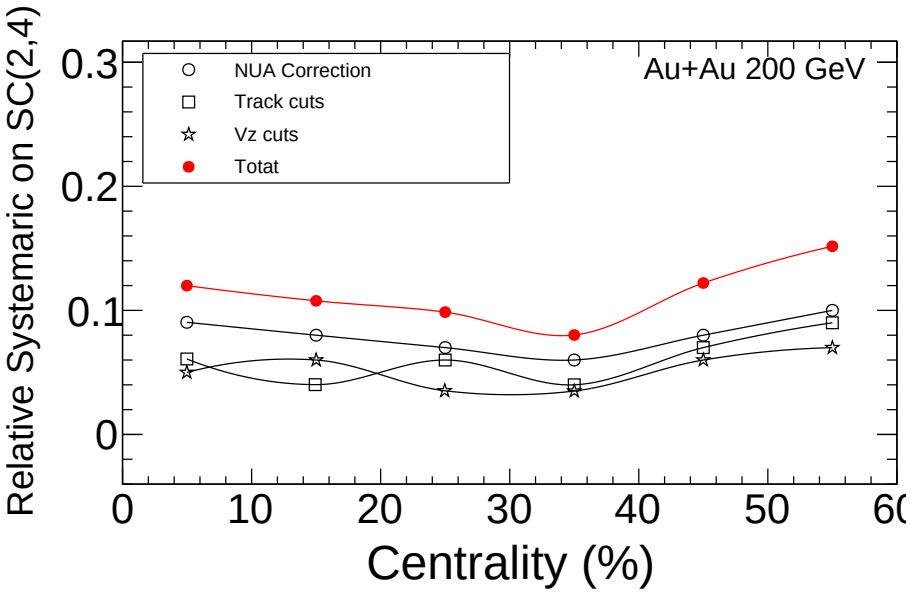

Figure 7: Relative systematic error on SC(2,4) at 200 GeV

5 RESULTS & DISCUSSION

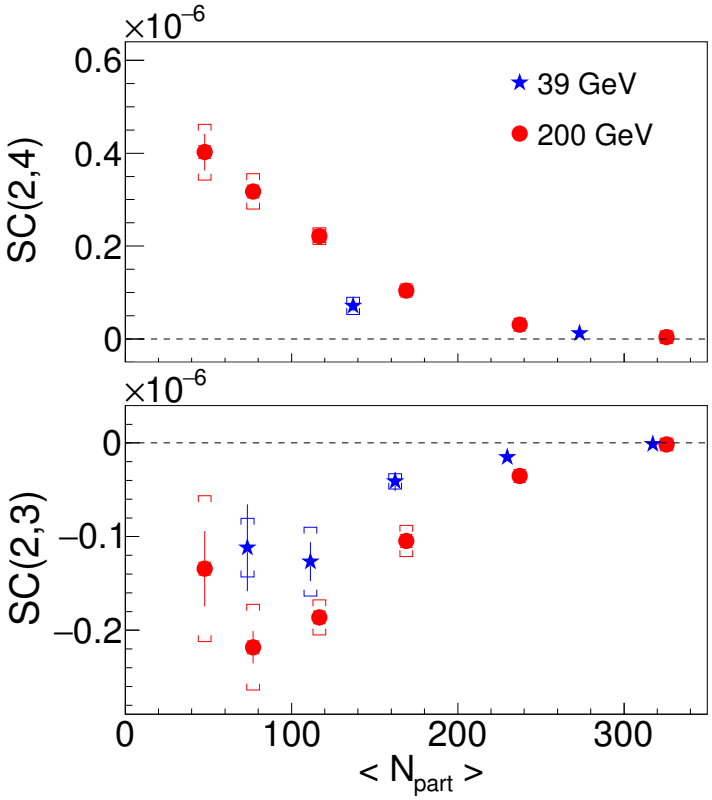

Figure 8: $SC(2,4)$ and $SC(2,3)$ as functions of $\langle N_{part} \rangle$ in Au+Au collision at $\sqrt{s_{NN}}$ = 39 and 200 GeV. Verticals lines are statistical uncertainties and systematic errors are shown with Cap symbols.

Figure 8 presents the symmetric cumulant $SC(2,3)$ and $SC(2,4)$ as functions of centrality (represented by the average number of participating nucleons, $\langle N_{part} \rangle$), at midrapidity ($|\eta| < 1.0$) for charged hadrons in Au+Au collision at $\sqrt{s_{NN}}$ = 39 and 200 GeV. Systematic errors are shown with Cap symbols. Positive values of $SC(2,4)$ are observed for all centrality intervals at both collision energies, suggestive of a correlation between v_2 and v_4. On the other hand, the negative values of $SC(2,3)$ reveal the anticorrelation between v_2 and v_3. The magnitude of the (anti)correlation increases from central to peripheral events at both collision energies. An inherent feature of the symmetric cumulant is the suppression of nonflow effects thanks to the use of the four-particle correlation. Nonflow refers to azimuthal correlations not related to the reaction plane orientation, arising from resonances, jets, quantum statistics, final-stage interactions like Coulomb effects, and so on. We have confirmed (using the HIJING model [26, 27]) that nonzero values of symmetric cumulants cannot be explained by nonflow effects.

A normalized symmetric cumulant will facilitate comparisons between different collision energies or between data and model calculations. The normalized symmetric cumulant $NSC(m,n)$ is defined in Eq. 4.

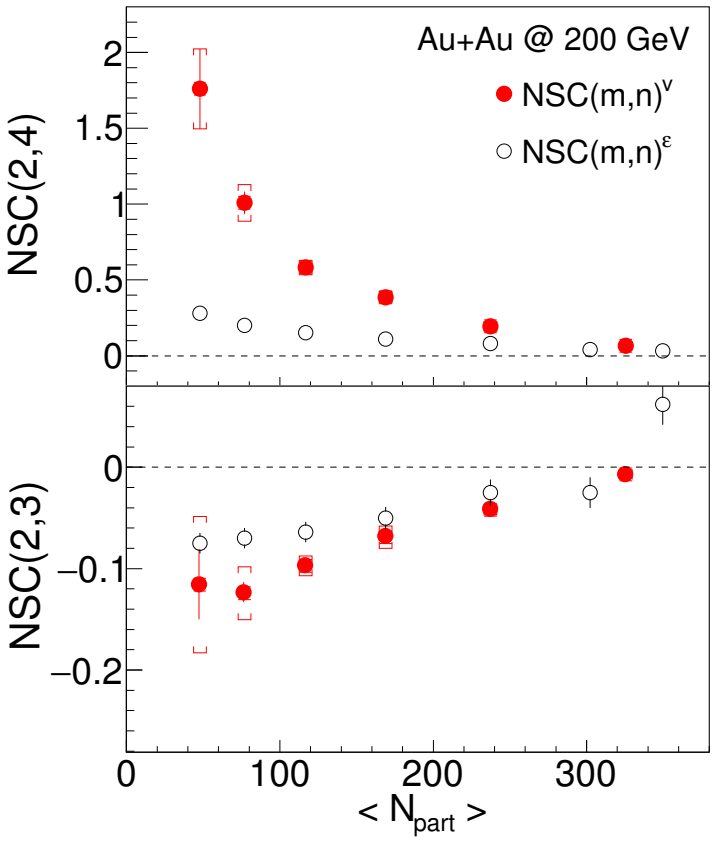

Figure 9: NSC(2,4) and NSC(2,3) as functions of $\langle N_{part} \rangle$ in Au+Au collision at $\sqrt{s_{NN}}$ = 200 GeV. The normalized symmetric cumulants evaluated in the coordinate space, $NSC(m,n)^{\varepsilon_m,\varepsilon_n}$, using the Glauber model is also shown.

Anisotropic flow is generated by the initial geometric anisotropy (and its fluctuations) coupled with an expansion of the produced medium. There is an intense interest in understanding the occurence of the initial-stage fluctuations and how these fluctuations propagate and manifest themselves in correlations between measured particles. The normalized symmetric cumulants evaluated in the coordinate space, $NSC(m,n)^{\varepsilon}$, in Au+Au collision at $\sqrt{s_{NN}}$ = 200 GeV (using the Monte Carlo Glauber model) is shown in Fig. 9 and compared with $NSC(m,n)^{v}$ measured in the momentum space. Figure 9 demonstrates that the initial-stage anticorrelation between the 2^{nd} (ε_2) and 3^{rd} (ε_3) order eccentricity is mainly responsible for the observed anticorrelation between v_2 and v_3. However, the correlation between ε_2 and ε_4 underpredicts the observed correlation between v_2 and v_4, leaving room for the medium properties to play a role, as suggested by model calculations [3, 24]. Therefore, NSC(2,4) provides a probe into the medium properties. The difference between $NSC(2,4)^{v}$ and $NSC(2,4)^{\varepsilon}$ increases from central to peripheral collisions, presumably because ε_2 has an increased contribution in v_4 in more peripheral collisions. This is consistent with the observation reported by ATLAS [29] and ALICE [2] experiments in Pb+Pb collisions at 2.76 TeV.

Fig. 10 shows the $\langle N_{part} \rangle$ dependence of the normalized symmetric cumulants NSC(2,4) and NSC(2,3) in Au+Au collision at $\sqrt{s_{NN}}$ = 39 (blue stars) and 200 GeV

(red circles). Ref. [28] shows that if NSC(m,n) is measured in a wide centrality range, where the impact parameter significantly fluctuates, the measurements of the symmetric cumulants will be biased by such fluctuations. This is known as the centrality bin width (CBW) effect. Accordingly, in this analysis the symmetric cumulants were measured in small multiplicity windows and then combined into 10% bins to reduce statistical uncertainties.

Figure 10 hints at an energy dependence of NSC$(2,4)$. The magnitude of NSC$(2,4)$ is systematically higher at the lower energy (39 GeV), though the observed difference is not statistically significant (a $\sim 2\sigma$ effect). This difference could be related to the change in the initial conditions and/or in the transport properties of the medium with collision energy. Future high-statistics measurements at low energies in the phase II of the Beam Energy Scan program (BES-II) at RHIC will further our understanding of the temperature dependence of η/s, since NSC$(2,4)$ is sensitive to the transport properties of the medium. The lower panel of Fig. 10 shows a comparison of NSC$(2,3)$ as a function of centrality between 39 GeV and 200 GeV. The results of NSC$(2,3)$ at 39 and 200 GeV are consistent with each other. In Fig. 10, the ALICE measurements for 2.76 TeV Pb+Pb [2] (gray bands) are also shown in comparison. Since the ALICE results have not been corrected for the CBW effect, we have also illustrated the STAR results without the CBW correction at 200 GeV (red bands) to make a fair comparison. There is a slight difference in NSC$(2,4)$ between results with and without the CBW correction; however this effect is larger in NSC$(2,3)$. The uncorrected values of NSC$(2,3)$ or NSC$(2,4)$ at 200 GeV and 2.76 TeV are very close to each other for all the centrality intervals.

We compare in Fig. 11 our measurements with available model predictions [24, 28] for NSC$(2,3)$ and NSC$(2,4)$ in Au+Au collisions at 200 GeV. The AMPT calculations [24] explore two scenarios with $\eta/s = 0.08$ and 0.18, respectively. In the AMPT model, η/s in a partonic matter is estimated with the assumption that the partonic matter only consists of noninteracting massless u and d quarks. The data of NSC$(2,3)$ are reasonably well described by the AMPT model with both $\eta/s = 0.08$ and 0.18. On the other hand, the NSC$(2,4)$ from AMPT depends on η/s, and the experimental data favor the calculations with $\eta/s = 0.18$. However, both scenarios underpredict the data. Predictions from an ideal hydrodynamics model (NexSPheRIO) [28] are shown with yellow bands in Fig. 11. The Ideal hydrodynamics model is able to explain the anti-correlation between v_2 and v_3, but underpredicts the correlation between v_2 and v_4. It is remarkable that the NexSPheRIO model describes reasonably well the magnitudes of all flow harmonics (v_2, v_3 and v_4) measured in all centrality intervals at the top RHIC energy. The failure of the ideal hydrodynamics model at the v_2-v_4 correlation supports the idea that the symmetric cumulants are more sensitive to the details of the theoretical calculations than the individual flow harmonics. Like the ideal hydrodynamics model, a viscous hydrodynamics model ($\eta/s = 0.08$) roughly explains the NSC$(2,3)$ data and underpredicts NSC$(2,4)$. However, the prediction from the viscous hydrodynamics model for NSC$(2,4)$ is much closer to data than the ideal hydrodynamics model.

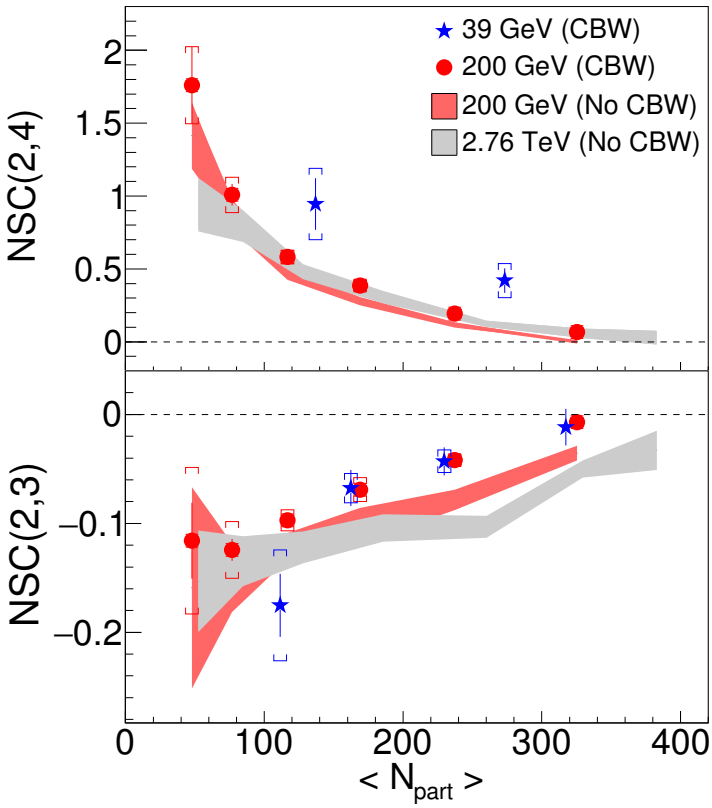

Figure 10: NSC(2,4) and NSC(2,3) as functions of average $\langle N_{part} \rangle$ in Au+Au collision at $\sqrt{s_{NN}}$ = 39 and 200 GeV. ALICE results for 2.76 TeV Pb+Pb [2] are also shown in comparison. Vertical lines are statistical uncertainties. Systematic errors are shown with Cap symbols. Results shown with markers have been corrected for the centrality bin width effect, whereas the bands represent results without such a correction.

6 APPENDIX I : NON-FLOW ESTIMATION

We have calculated the SC observables using HIJING [7] which does not include anisotropic collectivity but e.g. azimuthal correlations due to jet production. It is found that in HIJING both $\langle\langle\cos(m\varphi_1+n\varphi_2-m\varphi_3-n\varphi_4)\rangle\rangle$ and $\langle\langle\cos[m(\varphi_1-\varphi_2)]\rangle\rangle$ $\langle\langle\cos[n(\varphi_1-\varphi_2)$ are non-zero. However, the calculation of SC observables from HIJING are compatible with zero for all centralities (see Fig. 12 on page 14), which suggests that the SC measurements are nearly insensitive to non-flow correlations.

7 APPENDIX II : ENERGY DEPENDENCE OF NSC(2,4)

Fig. 13 shows energy dependence of NSC(2,4) at 0-20% centrality. Measurement below 39 GeV is limited by statistics. We see a hint of change in NSC(2,4) as a function of energy, NSC(2,4) at 39 GeV is higher than 200 GeV with 2σ confidence level. Measurement of NSC(2,4) in STAR BES -II programm will be useful to understand the

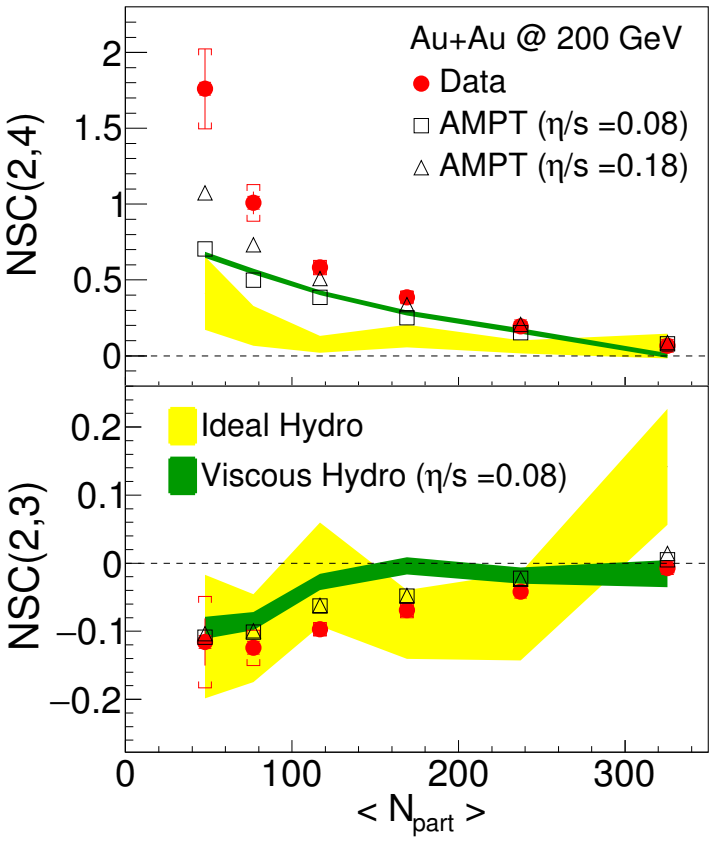

Figure 11: NSC(2,4) and NSC(2,3) as functions of average $\langle N_{part} \rangle$ in Au+Au collision at $\sqrt{s_{NN}}$ = 200 GeV, with hydrodynamics and AMPT model predictions in comparison.

energy dependence of NSC(2,4).

8 APPENDIX III : MODEL COMPARISON AT 39 GEV

Fig. 14 shows comparison between data and AMPT ($\eta/s = 0.18$) model at 39 GeV. Like 200 GeV, AMPT model explains SC(2,3) data. However a large difference between data and model prediction is observed. Hydro model prediction at 39 GeV is not available.

9 APPENDIX IV : CENTRALITY DETERMINATION (MULTIPLICITY VS IMPACT PARAMETER)

Fig. 15 shows comparison of SC(m,n) using two method of centrality selection in AMPT model. We have seen that use of multiplicity to determines centrality gives consistent results with the calculation using centrality from impact parameter.

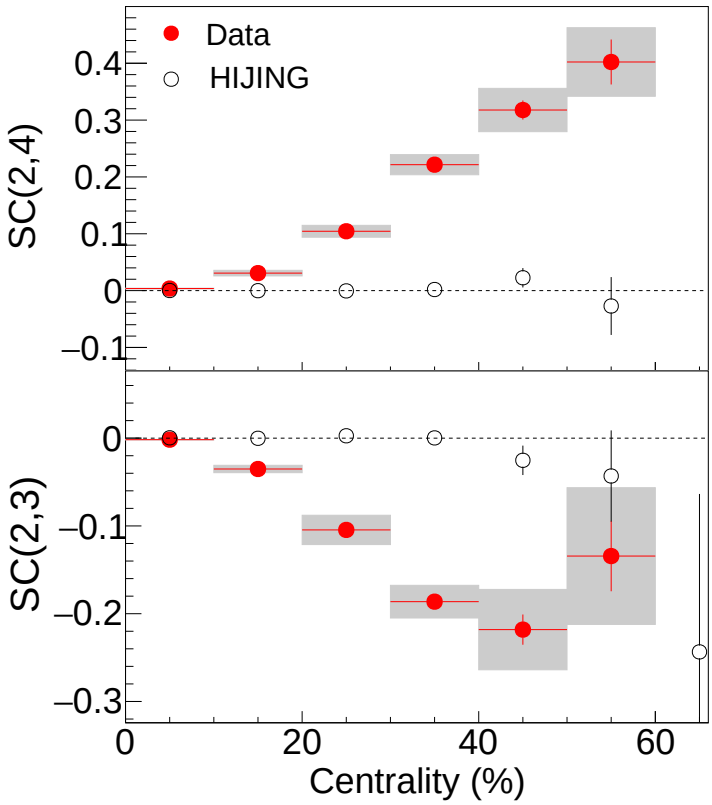

Figure 12: SC(2,3) and SC(2,4) as a function of centrality in Au+Au collision at 200 GeV from data and HIJING

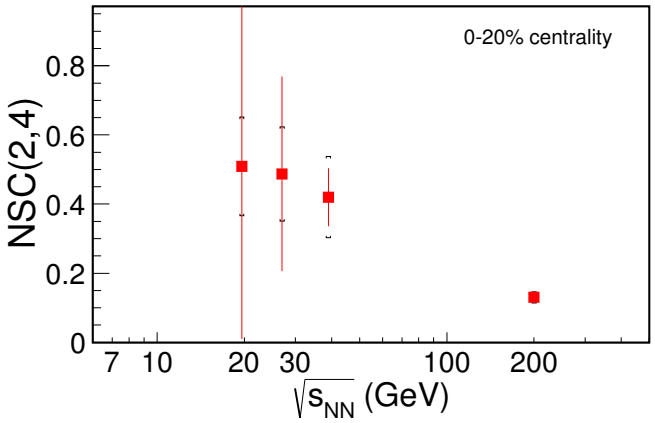

Figure 13: NSC(2,4) as a function of beam energy in Au+Au collision at 200 GeV.

REFERENCES

[1] A. Bilandzic *et al.*, Phys.Rev. **C 89**,064904 (2014).

[2] J. Adam *et al.*, (ALICE Collaboration) Phys. Rev. Lett. **117**, 182301 (2016).

[3] X. Zhu *et al.*, arXiv:1608.05305.

[4] Y. Zhou *et al.*, Phys. Rev. **C 93**, 034909 (2016).

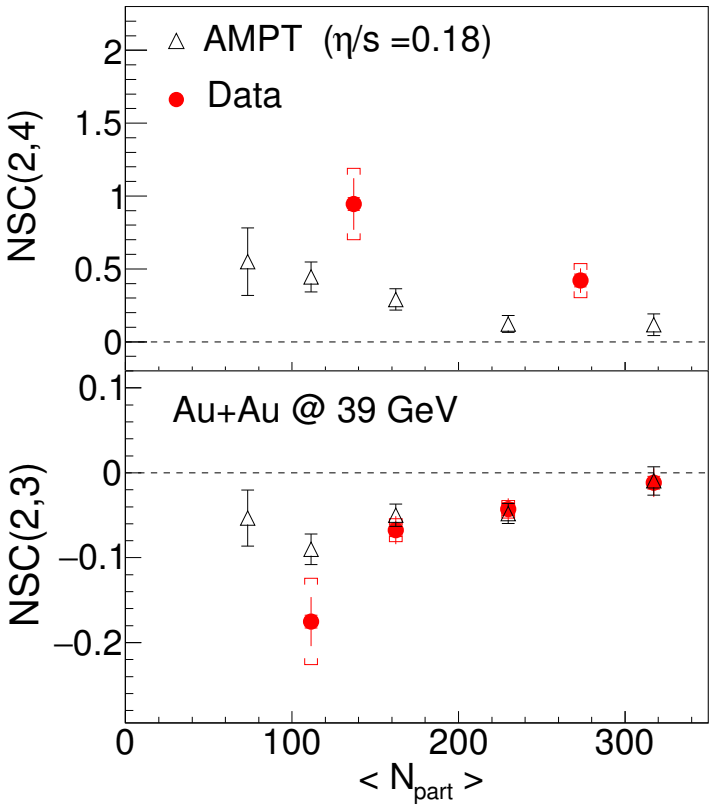

Figure 14: NSC(m,n) as a function of Npart in Au+Au collision at 39 GeV from data and AMPT model.

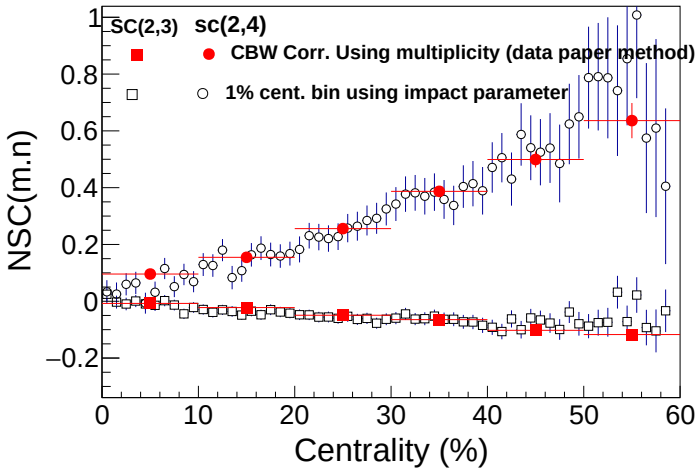

Figure 15: Comparison of SC(m,n) using two method of centrality selection in AMPT model

[5] F. G. Gardim *et al.* arXiv:1608.02982.

[6] Zi-Wei Lin and C. M. Ko, Phys. Rev. **C 65**, 034904 (2002);
Zi-Wei Lin *et al.*, Phys. Rev. **C 72**, 064901 (2005);
Lie-Wen Chen *et al.*, Phys. Lett. **B 605** 95 (2005).

[7] X. N. Wang and M. Gyulassy, Phys. Rev. **D 44**, 3501 (1991).

[8] B. Zhang, Comput. Phys. Commun. **109**, 193 (1998).

[9] R. S. Bhalerao and J.-Y Ollitrault, Phys. Lett. **B 641**, 260 (2006).

[10] R. S. Bhalerao *et al.* Phys. Lett. **B 627**, 49 (2005).

[11] D. Teaney, J. Lauret and E. V. Shuyak ,Phys. Rev. Lett. **86**, 4783 (2001).

[12] J.-Y. Ollitrault, Phys. Rev. **D 46**, 229 (1992).

[13] C. Adler *et al.*, (STAR Collaboration), Phys. Rev. Lett. **87**, 182301 (2001).

[14] A. M. Poskanzer and S. A. Voloshin, Phys. Rev. **C 58**, 1671 (1998).

[15] D. Teaney *et al.* Phys. Rev. Lett. **86**, 4783 (2001).

[16] P. F. Kolb *et al.* Phys. Lett. **B 500**, 232 (2001).

[17] H. Sorge, Phys. Rev. Lett. **78**, 2309 (1997).

[18] B. Zhang *et al.* Phys. Lett. **B 455**, 45 (1999).

[19] M. Miller, R. Snellings, arXiv:nucl-ex/0312008.

[20] B. Alver *et al.*, (PHOBOS Collaboration) Phys. Rev. Lett. **98**, 242302 (2007).

[21] G. Aad *et al.*, (ATLAS Collaboration) Phys. Rev. **C 90**, 024905 (2014).

[22] F. G. Gardin *et al.*, Phys. Rev. Lett. **109**, 202302 (2012).

[23] B. Schenke *et al.*, Phy. Rev. **C 85**, 024901 (2012).

[24] Md. Nasim , Phys. Rev. **C 95**, 034905 (2017).

[25] A. Bilandzic *et al.*, Phys. Rev. **C 83** 044913 (2011).

[26] M. Gyulassy and X. N. Wang, Comput. Phys. Commun. **83**, 307 (1994).

[27] X. N. Wang and M. Gyulassy, Phys. Rev. D **44**, 3501 (1991).

[28] F. G. Gardin *et al.*, Phys. Rev. **C 95**, 034901 (2017) and private communication.

[29] G. Aad *et al.*, (ATLAS Collaboration) Phys. Rev. **C 92**, 034903 (2015).